

# In vitro study of enhanced photodynamic cancer cell killing effect by nanometer-thick gold nanosheets

Ziyi Zhang<sup>1,§</sup>, Dalong Ni<sup>2,3,§</sup>, Fei Wang<sup>1</sup>, Xin Yin<sup>1</sup>, Shreya Goel<sup>2</sup>, Lazarus N. German<sup>1</sup>, Yizhan Wang<sup>1</sup>, Jun Li<sup>1</sup>, Weibo Cai<sup>2,3</sup> (), and Xudong Wang<sup>1</sup> ()

- <sup>1</sup> Department of Materials Science and Engineering, University of Wisconsin-Madison, Madison, Wisconsin 53706, USA
- <sup>2</sup> Department of Radiology, University of Wisconsin-Madison, Madison, Wisconsin 53705, USA
- <sup>3</sup> University of Wisconsin Carbone Cancer Center, Madison, Wisconsin 53705, USA

© Tsinghua University Press and Springer-Verlag GmbH Germany, part of Springer Nature 2020

Received: 8 October 2019 / Revised: 11 July 2020 / Accepted: 18 July 2020

#### **ABSTRACT**

Photodynamic therapy (PDT) by near-infrared (NIR) irradiation is a promising technique for treating various cancers. Here, we reported the development of free-standing wafer-scale Au nanosheets (NSs) that exhibited an impressive PDT effect. The Au NSs were synthesized by ionic layer epitaxy at the air-water interface with a uniform thickness in the range from 2 to 8.5 nm. These Au NSs were found very effective in generating singlet oxygen under NIR irradiation. *In vitro* cellular study showed that the Au NSs had very low cytotoxicity and high PDT efficiency due to their uniform 2D morphology. Au NSs could kill cancer cells after 5 min NIR irradiation with little heat generation. This performance is comparable to using 10 times mass loading of Au nanoparticles (NPs). This work suggests that two-dimensional (2D) Au NSs could be a new type of biocompatible nanomaterial for PDT of cancer with an extraordinary photon conversion and cancer cell killing efficiency.

### **KEYWORDS**

gold nanosheet, ionic layer epitaxy, surface plasmon, photodynamic effect, cancer therapy

#### 1 Introduction

Cancer is one of the deadliest diseases for human beings. Numerous research efforts have been implemented for cancer cell killing. Among all currently available treatments, photodynamic therapy (PDT) is an attractive technique for killing various cancer cells [1, 2]. It is a noninvasive procedure that involves light, photosensitizers and tissue oxygen, and causes minimal damage to surrounding tissues. It, therefore, induces minimal damage to human bodies and has fewer side effects comparing to surgery, chemotherapy and radiation therapy [3–5]. Near infrared (NIR) light is usually employed for PDT treatment because it has deep tissue penetration [6]. Nanomaterials that absorb NIR light and generate reactive oxygen species (ROS) are usually used as photosensitizers for PDT to kill cancer cells. Au nanoparticles (NPs) are well known for their chemical inertness and low cytotoxicity [7], and has been considered as a good candidate for PDT in cancer treatment [8, 9]. It has been reported that the morphologies of metal nanomaterials have a very strong influence on their optical properties and surface reactivity [10-14]. It was found that singlet oxygen (one of the ROS) can be generated by photoirradiation at the longitudinal bands, but not at the transverse band of Au nanorods [15]. Large surface area with large dimensions would enhance the surface plasmon resonance in longer wavelength range and promotes singlet oxygen generation. Therefore, an ultrathin sheet-like morphology could be a superior structure to increase the absorption of NIR and maximize the efficiency

of singlet oxygen generation. It is thus essential to investigate how the 2D morphology affects the metal nanomaterials' photophysical and photochemical properties and to study their application as a PDT photosensitizer in cancer treatment.

In this work, centimeter-sized ultrathin Au nanosheets (NSs) were synthesized using ionic layer epitaxy (ILE) method [16, 17]. The Au NSs exhibited a broad absorption in the visible light and NIR region. We further demonstrated that the Au NSs could generate singlet oxygen under NIR irradiation with minimal heat generation. These Au NSs had a smooth surface and showed very low toxicity to living cells. *In vitro* studies revealed the superior capability of the Au NSs in killing murine 4T1 breast cancer cells under the irradiation of 808 nm wavelength laser. The ultrathin nature of the Au NSs significantly increased the singlet oxygen generation efficiency by Au surface plasmon resonance under NIR radiation, which promoted it to be highly efficacious PDT materials for cancer treatments.

# 2 Experimental

# 2.1 Synthesis of 5 nm Au nanosheets

Au NSs were synthesized by ILE method. In a typical synthesis, 5 mL de-ionized (DI)  $H_2O$  was prepared in a 24-mL glass vial. Subsequently, 100  $\mu L$  2.857 mM L-arginine (L-arg, Sigma-Aldrich) aqueous solution and 30  $\mu L$  of 20 mM gold(III) chloride hydrate (HAuCl<sub>4</sub>-xH<sub>2</sub>O, Sigma-Aldrich) aqueous solution were added into the glass vial. Then, 8  $\mu L$  chloroform solution containing

<sup>§</sup> Ziyi Zhang and Dalong Ni contributed equally to this work.

1.8 mM oleylamine (Sigma-Aldrich) was slowly spread onto the precursor solution surface. Finally, this glass vial was screwcapped and was carefully transferred into a convection oven and kept at 60 °C for 180 min. The Au NSs could be transferred onto an arbitrary substrate by scooping at the surface of the solution or extracting solution from the bottom for characterization and device fabrication.

#### 2.2 Synthesis of 2, 4, 6, 8.5 nm Au nanosheets

Au NSs at different thickness were all synthesized by ILE method with various precursor concentrations and heating time lengths. For 2 nm Au NSs, 100 µL 2.857 mM L-arg solution and 30 μL of 20 mM HAuCl<sub>4</sub>·xH<sub>2</sub>O solution were added into 5 mL DI H2O. The solution was heated for 90 min at 60 °C. For 4 nm Au NSs, 200 µL 2.857 mM L-arg solution and 60 μL of 20 mM HAuCl<sub>4</sub>·xH<sub>2</sub>O solution were added into 5 mL DI H<sub>2</sub>O. The solution was heated for 90 min at 60 °C. For 6 nm Au NSs, 200 μL 2.857 mM L-arg solution and 60 μL of 20 mM HAuCl<sub>4</sub>·xH<sub>2</sub>O solution were added into 5 mL DI H<sub>2</sub>O. The solution was heated for 180 min at 60 °C. For 8.5 nm Au NSs,  $100\,\mu L$  2.857 mM L-arg solution and 30  $\mu L$  of 20 mM HAuCl<sub>4</sub> xH<sub>2</sub>O solution were added into 5 mL DI H<sub>2</sub>O. The solution was heated for 17 h at 60 °C.

#### 2.3 Characterization

A Zeiss LEO 1530 field-emission scanning electron microscope (FESEM) was used to study the morphologies of the Au NSs. Atomic force microscopy (AFM) tomography images were obtained using an XE-70 Park System. X-ray photoelectron spectroscopy (XPS) spectrum was obtained from a Thermo Scientific K-alpha XPS instrument at a 400 µm spot size, with the flood gun turned on during the measurements. FEI TF30 transmission electron microscope (TEM) operated at 300 kV was used to study the crystal structure. Ultraviolet-visiblenear-infrared (UV-vis-NIR) spectroscopy was performed on a Spectrometer UV-vis-NIR Lambda 19. In situ grazing incidence X-ray diffraction (GIXD) experiment was performed at beamline 15-ID-C ChemMatCARS at the Advanced Photon Source (APS) in Argonne National Laboratory.

#### 2.4 Singlet oxygen detection

Singlet oxygen sensor green (SOSG) was employed to evaluate the singlet oxygen generation of Au NSs. Au NSs of different thicknesses were transferred onto 15-mm diameter thin glass disk substrates, which were put to the bottom of a 24-well cell culture plate. 1 mL phosphate buffer saline (PBS) containing 0.15 µL SOSG was added to each sample. Then, they were irradiated with an NIR laser (808 nm, 3 W/cm<sup>2</sup>). The SOSG fluorescence was obtained from the ClarioStar Plate Reader with an excitation of 504 nm wavelength. The fluorescence result was quantified by comparing the SOSG fluorescence enhancement with the control samples of blank glass disks.

## 2.5 Measurements of singlet oxygen quantum yield

The measurements of singlet oxygen quantum yield  $(\Phi_{\Delta})$  were performed in ethanol with 1,3-diphenylisobenzofuran (DPBF) as the <sup>1</sup>O<sub>2</sub> indicator and methylene blue (MB) as the standard photosensitizer. The generation of singlet oxygen could be found by reduced absorption of the DPBF at 410 nm.  $\Phi_{\Delta}$  was calculated by  $\Phi_{\Delta}$  (sample) =  $\Phi_{\Delta}$ (MB)·m(sample)/m(MB), using the standard MB dye with known singlet oxygen quantum yield of  $\Phi_{\Delta} = 0.52$  (in ethanol) [18], where m represents the slope of a linear fit through plotting the natural logarithm of the reduction of the 410 nm DBPF band against the exposure time.

# 2.6 Cell culture and cytotoxicity assessment

Murine breast cancer 4T1 cells were cultured at 37 °C and with 5% CO2 in Roswell Park Memorial Institute medium (RPMI) 1640 supplemented with 1% penicillin/streptomycin and 10% fetal bovine serum (FBS). Human embryonic kidney 293 (HEK293) cells were obtained from the American Type Culture Collection (ATCC) and cultured under 5% CO2 at 37 °C in Dulbecco's Modified Eagle Medium (DMEM) supplemented with 1% penicillin/streptomycin and 10% FBS. Au NSs of different thicknesses were transferred onto 15-mm diameter thin glass substrates, which were put to the bottom of a 24-well cell culture plate. Cells were seeded into the 24-well cell culture plate at 10<sup>5</sup> per well and then incubated for 24 h at 37 °C under 5% CO<sub>2</sub>, and the cell viability was then measured by MTT assay.

### 2.7 In vitro photodynamic performance

For therapeutic experiments, an 808 nm laser irradiation at 3.0 W/cm<sup>2</sup> was applied in all cases. The Au NSs were rinsed with DI water and 75% ethanol solution before the in vitro experiment. To investigate the impact of gold morphology on photodynamic conversion, thermal evaporated gold nanofilms (Au NFs) at different thickness and 5 nm gold nanoparticle (Au NPs) solutions at different concentrations were all irradiated for 5 min.

#### Results and discussion

## 3.1 As-synthesized Au NSs from ILE method

The ultrathin Au NSs were synthesized via ILE at the air-water interface. The AuCl<sub>4</sub> precursor ions in the solution were attracted by a positively ionized oleylamine monolayer at the air-water interface, where they were reduced to Au<sup>0</sup> by L-arginine. When the solution was kept at 60 °C, Au nanocrystals nucleated and grew at the concentrated interface layer [19]. Guided by the rearrangement of oleylamine molecules, Au nanocrystals gradually formed into a uniform ultrathin 2D morphology covering the entire water surface. The as-synthesized Au NSs were floating at the water surface and were readily transferred to any arbitrary substrate. This synthesis was conducted in a 5-inch glass petri dish. By slowly extracting the solution, the Au NS was transferred onto a 4-inch Si wafer. As shown in the optical image (Fig. 1(a)), the as-transferred nanosheet almost fully covered the entire Si wafer with high uniformity.

The topography of this nanosheet was first characterized by SEM and AFM. After a 3-hour synthesis, the Au NSs were smooth and flat, with a uniform thickness of 5.0 nm and a roughness less than 0.4 nm (Figs. 1(b) and 1(c)). This result revealed that the nanosheet was a continuous single piece rather than a particle-assembled layer. Some Au NPs were found on the nanosheet surface. They were formed in the bulk solution phase and were picked up onto the nanosheet surface during sample transfer. They could be removed by gently rinsing the sample surface using DI water. TEM was implemented to investigate the crystallinity of the Au NSs. The lateral size of the nanosheets were too large to be fully imaged and a region at the center of the nanosheet was taken for the characterization. As shown in Fig. 1(d), the nanosheet was very flexible, some wrinkles were observed without cracks or particles. Selective area electron diffraction (SAED) pattern of this region gave a polycrystalline feature (Fig. 1(e)). The diffraction rings could be indexed to {111}, {200}, {220}, and {311} planes, which matched well with the face-center cubic structure of metal gold. High-resolution TEM (HRTEM) image (Fig. 1(f)) showed that the polycrystalline nanosheets had single crystalline domains

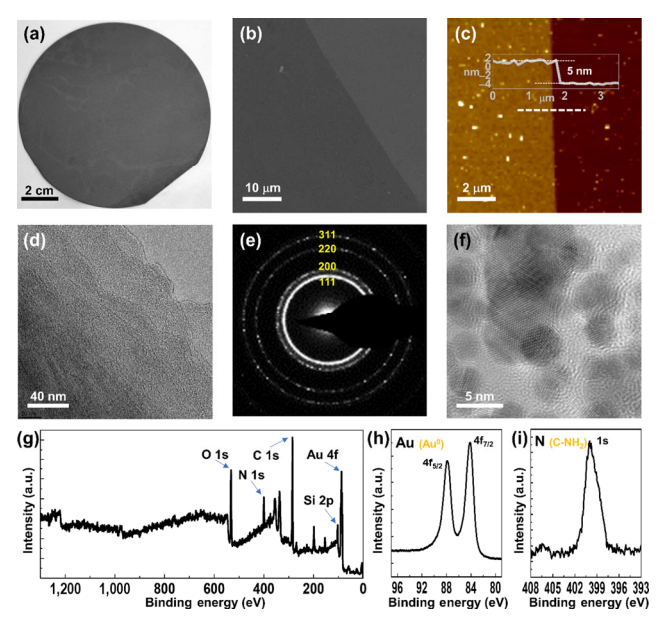


**Figure 1** Characterization of the gold nanosheets (Au NSs). (a) Optical image of Au NSs resting on a 4-inch Si wafer showing the excellent uniformity and scalability of the Au NSs. (b) SEM image and (c) AFM image of a nanosheet edge region on a Si substrate showing its topography and the thickness (the Au NSs are on the left-hand side). (d) TEM image and (e) the corresponding SAED pattern of (d). (f) HRTEM image of the Au NSs indicating a polycrystalline structure. (g)–(i) XPS elemental spectra: survey (g), Au 4f, (h) and N 1s (i), showing the zero valance Au and the presence of oleylamine on the metal Au NS.

of a few nanometers in sizes. In addition, the crystal evolution of Au NSs were further investigated using *in situ* GIXD. The measured GIXD spectrum was plotted as contour plots of the intensity as a function of both the horizontal  $(Q_{xy})$  and the vertical  $(Q_z)$  scattering vector components (Fig. S1 in the Electronic Supplementary Material (ESM)). The lattice spacing d was obtained from the in-plane diffraction data as  $d = 2\pi/Q_{xy}$  [20, 21]. The only diffraction pattern was a Bragg rod with  $Q_{xy}$  = 2.65 Å<sup>-1</sup>, giving a lattice spacing d = 2.37 Å that was corresponding to the Au (111) planes. This GIXD result confirmed that the Au NS was epitaxially-grown at the air–water interface into a two-dimensional (2D) morphology.

XPS was implemented to investigate the elemental characteristics and the bonding states of the Au NSs. A full wavelength survey scan showed multiple strong element signals from Au at 84.18 and at 87.88 eV, Si 2p at 103.08 eV, C 1s at 285.08 eV, N 1s at 399.98 eV, and O 1s at 533.08 eV (Fig. 1(g)). The signals of Si and O were from the bottom  $\text{SiO}_2$  substrate as the detective depth of XPS was longer than the thickness of the nanosheet. In the Au 4f fine scan shown in Fig. 1(h), the only two Au 4f peaks matched well with the chemical state of  $\text{Au}^0$ , where Au  $4f_{7/2}$  at 84.18 eV and  $4f_{5/2}$  at 87.88 eV. This

suggested that the  $AuCl_4^-$  was fully reduced by L-arginine and the formation of the metallic gold nanosheet. The single peak located at 399.98 eV in the N 1s spectrum matched the chemical state of N of C-NH<sub>2</sub> (Fig. 1(i)). This confirmed the existence of oleylamine, indicating the surfactant layer was remaining on the Au NSs.

# 3.2 Optical properties of Au NSs dependent on nanosheet thickness

In the ILE of Au NSs, the Au precursor was reduced by the reducing agent from the aqueous solution. Therefore, the thickness of these Au NSs could be rationally controlled by tuning the precursor concentrations and reaction time. Through this strategy, Au NSs with thickness varied from 2 to 8.5 nm were obtained. The Au NSs at different thickness were subjected to SEM and AFM analyses (Fig. S2 in the ESM). Compared to the 5 nm thickness obtained from the 3-hour synthesis, reducing the reaction time to 1.5-hour yielded 2 nm Au NSs; while increasing the reaction time to 17-hour gave the maximum thickness of 8.5 nm. This result showed that with enough precursors in the solution, longer reaction time would yield thicker Au NSs. Besides, by doubling the precursor concentrations, the 1.5-hour and 3-hour syntheses gave 4 and 6 nm Au NSs, respectively. These findings suggested that higher precursor concentration could raise the reaction rate leading to thicker nanosheets. While these nanosheets were all flat and uniform, the thinnest (2 nm) and the thickest (8.5 nm) Au NSs had the largest amount of nanoparticles spreading on the surface. For the thin nanosheet case, it was due to the fast nucleation rate within the electrical double layer, and thus the lateral growth was suppressed to form smooth nanosheets at the confined air-water interface region. For the thick nanosheet case, the nanosheet thickness was beyond the electrical double layer thickness and more reaction in the bulk solution phase provided more particles attached to the nanosheet. Within an optimal concentration and reaction time window, clean Au NSs with very little NPs could be obtained, such as the 5 nm Au NSs case.

For PDT applications, the materials must show desired NIR absorption capability. Thus, optical properties of Au NSs were investigated by UV-vis-NIR spectroscopy. Single layer Au NSs at different thickness all showed strong broad absorptions in the visible and NIR range (Fig. 2(a)). The absorbance intensity displayed a positive correlation with the Au NSs thickness. There was also a blue shift in the maximum absorption wavelength with decreasing Au NSs thickness [22, 23]. Figure 2(b) shows the normalized absorption spectra by the nanosheet thickness, revealing that thinner Au NSs had stronger absorption across the visible range, indicating that the light absorption was mainly at the nanosheet surface as a result of surface plasmon resonance. In the NIR region, 5 nm Au NS has the highest absorbance

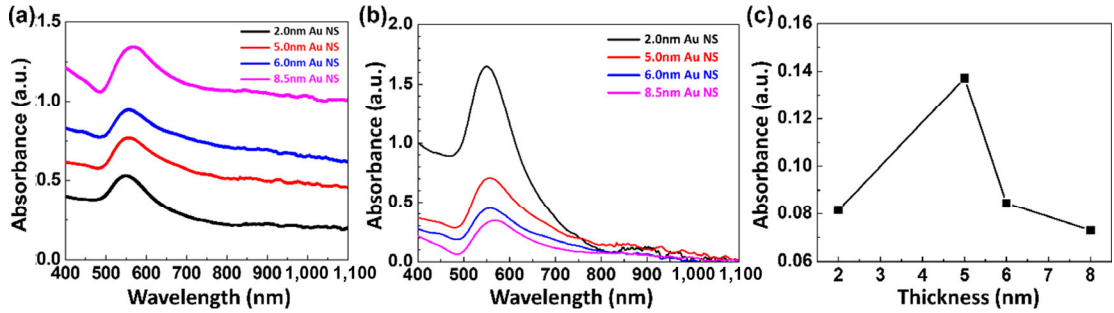


Figure 2 The optical properties of the Au NSs. (a) UV-vis-NIR absorption spectra of Au NSs at different thicknesses, showing a red-shifting of absorption peak as the Au NS thickness increases. (b) Normalized absorption spectra in (a) by Au NS thickness, revealing that the resonance is localized at the surface. (c) Absorbances at 808 nm wavelength in (b) indicate that 5 nm is the most efficient thickness for Au NS to absorb NIR wavelength.

than other thicknesses. This suggested that the major surface plasmon resonance region of absorbing NIR light is slightly deeper than that of visible light. At 808 nm wavelength, it's roughly in the depth of 2.5 nm beneath the surface, 5 nm Au NS had almost twice the absorbance compared to the other three nanosheet thicknesses (Fig. 2(c)).

# 3.3 In vitro Au NSs mediated photoirradiation cancer treatment

These outstanding optical properties of the Au NSs inspired us to use them for photoirradiation cancer treatment. As a proof-of-concept study, we carried out *in vitro* cellular experiments in order to evaluate the cancer cells killing effect of the Au NSs. The *in vitro* experiments were performed with 4T1 murine breast cancer cells on the Au NSs. As-synthesized 5 nm Au NSs were transferred on 1.5-mm diameter glass disks and cells were grown on the surface. Similar to the Si substrate, the glass disks were almost fully covered with a single layer of the nanosheet. Only a few micro cracks appeared on the nanosheet

surface, but this was negligible to change the nanosheets morphology and surface area. Cell culture medium containing normal cells (HEK293 cells) and cancer cells (4T1 cells) was individually added into 24-well plates (10<sup>5</sup> per well) with the Au NSs at the bottom. After 24 h incubation to allow the cells stick onto Au NSs, without applying laser irradiation, both normal cells and cancer cells showed over 90% viabilities on Au NSs (Figs. S3 and S4 in the ESM), except the cancer cells on 8.5 nm Au NSs. This lower viability from the 8.5 nm-thick nanosheet group was due to the rougher surface and more adsorbed Au NPs to thinner nanosheets. The adsorbed Au NPs may become toxic by penetrating the cell membrane and involving the reactions in the cells [24, 25].

To carry out the photoirradiation therapy, all cancer cells groups were irradiated with 808 nm laser at 3 W/cm² for 5 min (Fig. 3(a)). Optical images shown in Fig. 3(b) are the 4T1 cancer cells stained by trypan without or with the photoirradiation. Before irradiation, cancer cells are all alive in all groups with different Au NSs thicknesses. After 5 min

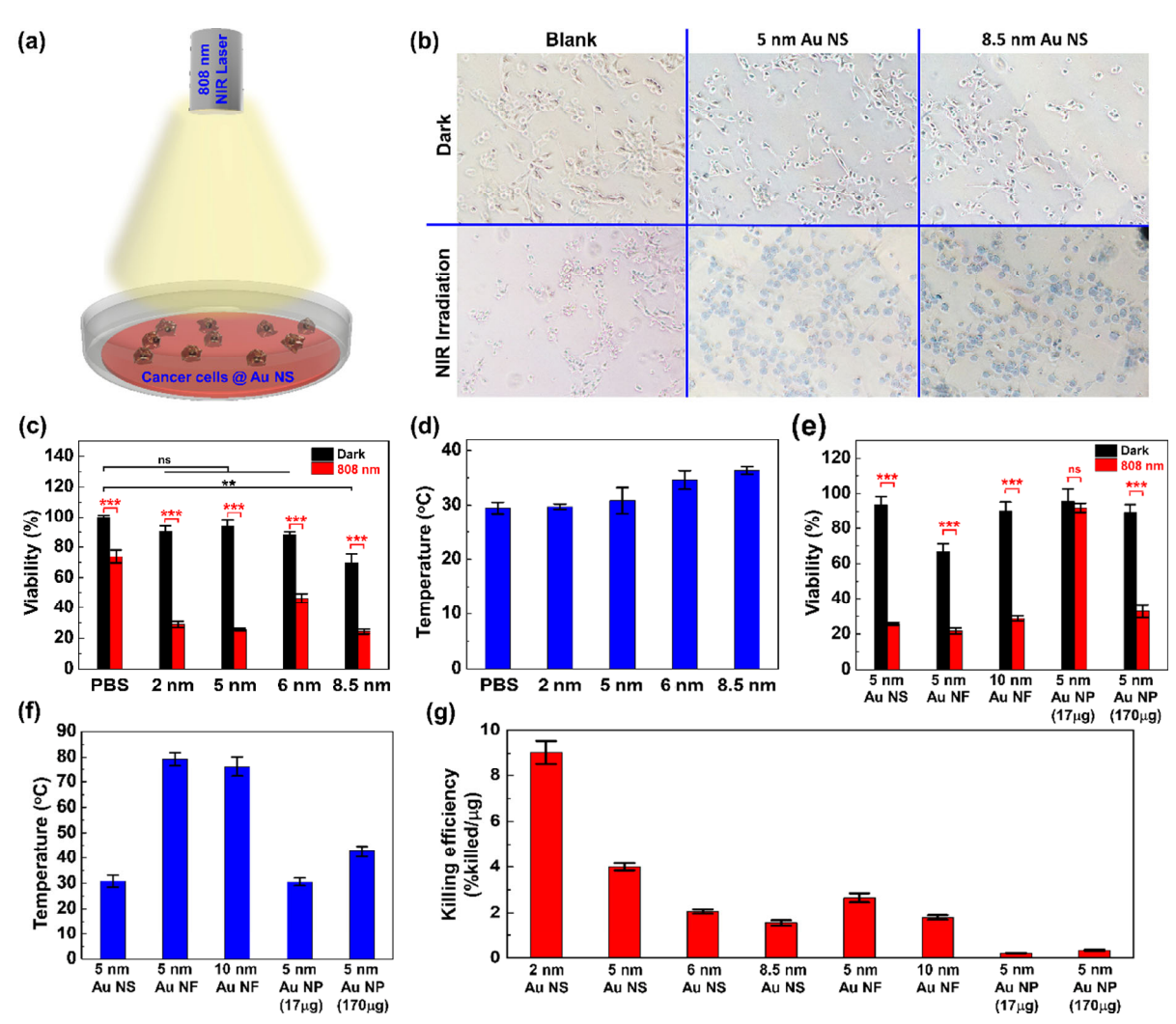
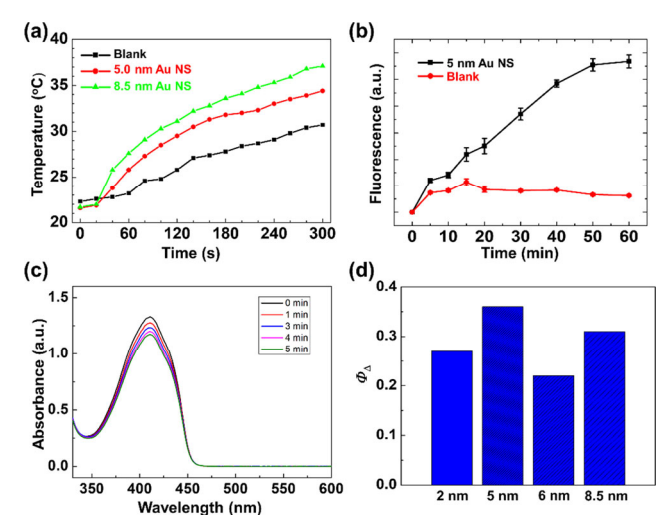


Figure 3 In vitro photoirradiation therapy for cancer cells killing by Au NSs. (a) Schematic illustration of the photodynamic therapy carried out by the Au NSs. Murine 4T1 breast cancer cells on the Au NSs were exposed to 808 nm laser (3 W/cm²) for 5 min. (b) Optical images of cancer cells stained by trypan blue without (Dark) or with the NIR irradiation. Cancer cells were alive in the dark on the bare glass and Au NSs, and the cells density was higher on the Au NSs region comparing to the bare glass region. Most of the cells on the Au NSs died after NIR irradiation while most of the cells on the glass were still alive. Cancer cell viabilities and temperature change in the Au NSs PDT. (c) Cancer cells viabilities on the Au NSs in the dark and after NIR irradiation, showing the cancer cells killing abilities of Au NSs via NIR irradiation. (d) The temperatures of the cancer cells after 5 min 808 nm laser irradiation (3 W/cm²). The temperature increases were too little to stimulate photothermal effect, suggesting a dominating photodynamic effect. (e) Cancer cells viabilities and (f) temperature of different Au nanostructures loaded with cancer cells after NIR irradiation (808 nm, 5 min at 3 W/cm²). The cancer cells died due to photothermal effect with all of the other Au nanostructures, except Au NSs. (g) Comparison of cancer cells killing efficiency normalized by sample mass, showing the superior PDT efficacy of Au NSs (P values for the viabilities were calculated by two-tailed test, ns P > 0.05; \* P < 0.05; \*

irradiation, cancer cells were still alive on the bare glass, but the majority of the cells were killed on the Au NSs. This result proved that Au NSs have the ability to kill cancer cells under NIR photoirradiation. Furthermore, cancer cell viability was also measured by a standard MTT assay and the result was summarized in Fig. 3(c). Using the PBS buffer as a control, Au NSs at different thickness all showed strong ability to kill cancer cells, and the 5 nm-thick nanosheet gave the best performance, more than 75% of the cancer cells were killed in 5 min. The temperature was also measured during the irradiation, which was slightly increased due to the photothermal effect of Au NSs. The temperature was higher with thicker nanosheets (Fig. 3(d)). However, none of the samples reached a temperature above 35 °C, which is not high enough for photothermal therapy (PTT). This fact suggested that the cancer cells were not killed by the photothermal effect of Au NSs. Besides, we conducted the cancer cells experiments with a lower power density of 1.5 W/cm<sup>2</sup>. The cell viabilities were increased in all groups after NIR irradiation. Although the PDT effect at lower power density is weaker, the cancer cell killing performance exhibited the same thickness dependence as the 3 W/cm<sup>2</sup> experiments, where 5 nm Au NSs showed the highest efficiency (Fig. S4 in the ESM). To understand the dominant effect causing the cell death, temperature was measured in PBS solutions without cancer cells (Fig. 4(a) and Fig. S5 in the ESM). The increased temperature was positively related to the thickness of the Au NSs, but the temperatures in the 5 min never reached 42 °C, which is the lower temperature threshold for PTT. These results excluded PTT as a possible major effect of cancer cell killing.

# 3.4 Improved PDT performance from Au 2D morphology

Therefore, we hypothesize that the PDT effect might played the key role for cancer cell killing as a result of singlet oxygen generated by Au NSs under NIR irradiation. To confirm that the Au NSs can indeed sensitize the formation of singlet oxygen upon photoirradiation, we added the commercial SOSG into the PBS solution before NIR irradiation. The nonfluorescent SOSG has been demonstrated to have a very good selectivity towards singlet oxygen, but is inert to hydroxyl radicals or superoxide [26-28]. Upon reaction with singlet oxygen to form endoperoxide, it becomes fluorescent and emits green fluorescence with a maximum at 525 nm. According to the result shown in Fig. 4(b), with the presence of Au NSs, a much stronger fluorescence signal was detected upon irradiation with 808 nm light comparing to the blank PBS group, thus indicating that photoirradiation with 808 nm light does generate singlet oxygen at the Au NSs surface. We also used a colorimetric method based on MB-bleaching after hydroxyl radical trapping to determine the generation of other ROS [29, 30]. We compared the ·OH generation of the Au NS in water to a control experiment without Au NS. No significant difference was found (Fig. S6 in the ESM), indicating a negligible generation of ·OH during irradiation. Importantly, the generation of singlet oxygen was further confirmed by using DPBF as the singlet oxygen indicator. The absorbance intensity of DPBF decreased significantly upon the exposure of DPBF to NIR in the presence of NSs for 5 min (Fig. 4(c)), confirming the quick production of singlet oxygen during the PDT process. In addition, the quantum yield  $(\Phi_{\Delta})$  of singlet oxygen was performed in ethanol solution with DPBF as the singlet oxygen indicator and MB as the standard photosensitizer. As the results summarized in Fig. 4(d), 5 nm Au NSs had the highest



**Figure 4** Photodynamic effect type determination and singlet oxygen yield measurement. (a) Temperature profiles of Au NSs during 5 min NIR irradiation, showing a trivial photothermal effect. (b) Fluorescence intensity of SOSG with 5 nm Au NS during 60 min NIR irradiation. Large amount singlet oxygen was generated on the Au NSs compared to on the bare glass. (c) Time-dependent absorption spectra of the DPBF in the presence of NSs upon exposure to NIR irradiation, confirming the generation of singlet oxygen. (d) The yield measurement of  ${}^{1}O_{2}$  using DPBF as the  ${}^{1}O_{2}$  indicator and methylene blue (MB) as the standard photosensitizer.

yield among the four thicknesses, which was consistent with the absorption spectra and PDT effects. The ROS generation study proved that the cancer cells were killed by the singlet oxygen generated from Au NSs. The Au NSs synthesized via ILE method do not require other surface modification with any functional materials.

In addition, we performed cellular experiments with other Au nanostructures as comparisons. Thermal evaporated Au NFs and 5 nm Au NPs were used for such comparison (Fig. S7 in the ESM). The cell viability results and temperature increases are shown in Figs. 3(e) and 3(f). To achieve a comparable cancer cell killing efficiency, the temperature with other nanostructures all went above 42 °C, which was typical for PTT effect. Thermal evaporated 5 nm Au NFs had a larger roughness comparing to 5 nm Au NSs and showed a much higher cytotoxicity. 5 nm Au NPs with the same mass loading (~ 17 μg) generated a similar heat from PTT effect and didn't show a strong ability to kill cancer cells. To enable PTT with Au NPs, at least 10 times mass loading was required (~ 170 μg) and Au NPs required about one day of incubation to enter the cells. The cancer cell killing efficiency was calculated by dividing the killing percentage over microgram, and this was shown in Fig. 3(g). The result revealed that ILE Au NSs are highly effective PDT materials, and their performances are much better than the PTT effect from other Au nanomaterials. The uniform 2D morphology of Au NSs promoted the absorption of NIR photon energy to generate singlet oxygen. The efficiency increases as the thickness decreases, suggesting that the PDT effect was given by the surface plasma property of the Au NSs. Without introducing additional photosensitizers, 5 nm Au NSs (~ 17 μg) were still able to yield an outstanding killing efficiency of 75% in 5 min under 3 W/cm<sup>2</sup> 808 nm laser irradiation, which is at the forefront of various Au nanomaterials reported in Refs. [31-37].

# 4 Conclusion

In summary, we reported an approach to prepare wafer-scale uniform Au NSs with a few nanometer thickness using ILE method with oleylamine monolayer as a surfactant template at

air-water interface. The nanosheet thickness could be controlled by tuning the precursor concentrations and reaction time. These Au NSs exhibited a broad absorption from the visible light to the NIR region and a strong singlet oxygen generation upon 808 nm photoirradiation rather than heat generation. It also has very low toxicity to living cells. Based on these unique properties, we have demonstrated *in vitro* cellular experiments showing that the ILE grown Au NSs are effective materials for cancer cells killing via PDT. The small temperature increases also showed that the PDT effect mediated by Au NSs is far more selective than their PTT effect. Moreover, the uniform 2D morphology of the Au NSs grown from the ILE technique achieved the highest cell killing efficiency among various Au nanostructures. With the structural advantages of Au NS, it could be made into plaster to treat skin cancers or salve to promote cleaning and healing the wound region after tumor cutting surgery. Au NS will be a very promising nanomaterial for PDT and will bring a new path to use large-area ultrathin 2D nanomaterials for medical treatments.

# Acknowledgements

This work was supported by the Army Research Office (No. W911NF-16-1-0198), the National Science Foundation (No. DMR-1709025), and National Institutes of Health (Nos. R01EB0213360, 1R21EB027857, and P30CA014520). Diffraction data was collected at ChemMatCARS Sector 15, which is principally supported by the Divisions of Chemistry and Materials Research, National Science Foundation, under grant number NSF/CHE-1834750. Use of the Advanced Photon Source, an Office of Science User Facility operated for the U.S. Department of Energy (DOE) Office of Science by Argonne National Laboratory, was supported by the U.S. DOE (No. DE-AC02-06CH11357).

Electronic Supplementary Material: Supplementary material (Au NSs characterizations, ROS measurements and ex situ cellular experiments) is available in the online version of this article at https://doi.org/10.1007/s12274-020-2990-7.

# References

- [1] Dolmans, D. E. J. G. J.; Fukumura, D.; Jain, R. K. Photodynamic therapy for cancer. Nat. Rev. Cancer 2003, 3, 380-387.
- Castano, A. P.; Mroz, P.; Hamblin, M. R. Photodynamic therapy and anti-tumour immunity. Nat. Rev. Cancer 2006, 6, 535-545.
- Cosgarea, R.; Susan, M.; Crisan, M.; Senila, S. Photodynamic therapy using topical 5-aminolaevulinic acid vs. surgery for basal cell carcinoma. J. Eur. Acad. Dermatol. Venereol. 2013, 27, 980-984.
- Lee, P. K.; Kloser, A. Current methods for photodynamic therapy in the US: Comparison of MAL/PDT and ALA/PDT. J. Drugs Dermatol. **2013**, 12, 925-930.
- Rhodes, L. E.; de Rie, M. A.; Leifsdottir, R.; Yu, R. C.; Bachmann, I.; Goulden, V.; Wong, G. A.; Richard, M. A.; Anstey, A.; Wolf, P. Five-year follow-up of a randomized, prospective trial of topical methyl aminolevulinate photodynamic therapy vs surgery for nodular basal cell carcinoma. Arch. Dermatol. 2007, 143, 1131-1136.
- Weissleder, R. A clearer vision for in vivo imaging. Nat. Biotechnol. 2001, 19, 316-317.
- Connor, E. E.; Mwamuka, J.; Gole, A.; Murphy, C. J.; Wyatt, M. D. Gold nanoparticles are taken up by human cells but do not cause acute cytotoxicity. Small 2005, 1, 325-327.
- [8] Cheng, Y.; Samia, A. C.; Meyers, J. D.; Panagopoulos, I.; Fei, B. W.; Burda, C. Highly efficient drug delivery with gold nanoparticle vectors for in vivo photodynamic therapy of cancer. J. Am. Chem. Soc. 2008, 130, 10643-10647.
- Hone, D. C.; Walker, P. I.; Evans-Gowing, R.; FitzGerald, S.; Beeby, A.; Chambrier, I.; Cook, M. J.; Russell, D. A. Generation of cytotoxic

- singlet oxygen via phthalocyanine-stabilized gold nanoparticles: A potential delivery vehicle for photodynamic therapy. Langmuir 2002, 18, 2985-2987.
- [10] Burda, C.; Chen, X. B.; Narayanan, R.; El-Sayed, M. A. Chemistry and properties of nanocrystals of different shapes. Chem. Rev. 2005, 105, 1025-1102.
- [11] Chen, H. J.; Ming, T.; Zhao, L.; Wang, F.; Sun, L. D.; Wang, J. F.; Yan, C. H. Plasmon-molecule interactions. Nano Today 2010, 5, 494-505
- [12] Sapsford, K. E.; Berti, L.; Medintz, I. L. Materials for fluorescence resonance energy transfer analysis: Beyond traditional donor-acceptor combinations. Angew. Chem., Int. Ed. 2006, 45, 4562-4589.
- [13] Haiss, W.; Thanh, N. T. K.; Aveyard, J.; Fernig, D. G. Determination of size and concentration of gold nanoparticles from UV-Vis spectra. Anal. Chem. 2007, 79, 4215-4221.
- [14] Foss, Jr., C. A.; Hornyak, G. L.; Stockert, J. A.; Martin, C. R. Template-synthesized nanoscopic gold particles: Optical spectra and the effects of particle size and shape. J. Phys. Chem. 1994, 98, 2963-2971.
- [15] Vankayala, R.; Kuo, C. L.; Sagadevan, A.; Chen, P. H.; Chiang, C. S.; Hwang, K. C. Morphology dependent photosensitization and formation of singlet oxygen  $(^{1}\Delta_{g})$  by gold and silver nanoparticles and its application in cancer treatment. J. Mater. Chem. B 2013, 1, 4379-4387
- [16] Wang, F.; Seo, J. H.; Luo, G. F.; Starr, M. B.; Li, Z. D.; Geng, D. L.; Yin, X.; Wang, S. Y.; Fraser, D. G.; Morgan, D. et al. Nanometrethick single-crystalline nanosheets grown at the water-air interface. Nat. Commun. 2016, 7, 10444.
- [17] Yin, X.; Chen, Q. Y.; Tian, P.; Zhang, P.; Zhang, Z. Y.; Voyles, P. M.; Wang, X. D. Ionic layer epitaxy of nanometer-thick palladium nanosheets with enhanced electrocatalytic properties. Chem. Mater. 2018, 30,
- [18] Redmond, R. W.; Gamlin, J. N. A compilation of singlet oxygen yields from biologically relevant molecules. Photochem. Photobiol.gy **1999**, 70, 391–475.
- [19] Yin, X.; Shi, Y. Q.; Wei, Y. B.; Joo, Y.; Gopalan, P.; Szlufarska, I.; Wang, X. D. Unit cell level thickness control of single-crystalline zinc oxide nanosheets enabled by electrical double-layer confinement. Langmuir 2017, 33, 7708-7714.
- [20] Jacquemain, D.; Wolf, S. G.; Leveiller, F.; Deutsch, M.; Kjaer, K.; Als-Nielsen, J.; Lahav, M.; Leiserowitz, L. Two-dimensional crystallography of amphiphilic molecules at the air-water interface. Angew. Chem., Int. Ed. 1992, 31, 130-152.
- [21] Jacquemain, D.; Leveiller, F.; Weinbach, S. P.; Lahav, M.; Leiserowitz, L.; Kjaer, K.; Als-Nielsen, J. Crystal structure of self-aggregates of insoluble aliphatic amphiphilic molecules at the air-water interface. An X-ray synchrotron study. J. Am. Chem. Soc. 1991, 113, 7684-7691.
- [22] He, Y. Q.; Liu, S. P.; Kong, L.; Liu, Z. F. A study on the sizes and concentrations of gold nanoparticles by spectra of absorption, resonance Rayleigh scattering and resonance non-linear scattering. Spectrochim. Acta Part A: Mol. Biomol. Spectrosc. 2005, 61, 2861-2866.
- [23] Chen, Y.; Gu, X.; Nie, C. G; Jiang, Z. Y.; Xie, Z. X.; Lin, C. J. Shape controlled growth of gold nanoparticles by a solution synthesis. Chem. Commun. 2005, 4181-4183.
- [24] Wang, S. G.; Lu, W. T.; Tovmachenko, O.; Rai, U. S.; Yu, H. T.; Ray, P. C. Challenge in understanding size and shape dependent toxicity of gold nanomaterials in human skin keratinocytes. Chem. Phys. Lett.
- [25] Choi, K.; Riviere, J. E.; Monteiro-Riviere, N. A. Protein corona modulation of hepatocyte uptake and molecular mechanisms of gold nanoparticle toxicity. Nanotoxicology 2017, 11, 64-75.
- [26] Flors, C.; Fryer, M. J.; Waring, J.; Reeder, B.; Bechtold, U.; Mullineaux, P. M.; Nonell, S.; Wilson, M. T.; Baker, N. R. Imaging the production of singlet oxygen in vivo using a new fluorescent sensor, Singlet Oxygen Sensor Green®. J. Exp. Bot. 2006, 57, 1725-1734.
- [27] Gollmer, A.; Arnbjerg, J.; Blaikie, F. H.; Pedersen, B. W.; Breitenbach, T.; Daasbjerg, K.; Glasius, M.; Ogilby, P. R. Singlet Oxygen Sensor Green®: Photochemical behavior in solution and in a mammalian cell. Photochem. Photobiol. 2011, 87, 671-679.
- [28] Ragàs, X.; Jiménez-Banzo, A.; Sánchez-García, D.; Batllori, X.;

Nonell, S. Singlet oxygen photosensitisation by the fluorescent probe Singlet Oxygen Sensor Green<sup>®</sup>. *Chem. Commun.* **2009**, 2920–2922.

- [29] Satoh, A. Y.; Trosko, J. E.; Masten, S. J. Methylene blue dye test for rapid qualitative detection of hydroxyl radicals formed in a fenton's reaction aqueous solution. *Environ. Sci. Technol.* 2007, 41, 2881– 2887.
- [30] Zhang, C.; Zhao, K. L.; Bu, W. B.; Ni, D. L.; Liu, Y. Y.; Feng, J. W.; Shi, J. L. Marriage of scintillator and semiconductor for synchronous radiotherapy and deep photodynamic therapy with diminished oxygen dependence. *Angew. Chem., Int. Ed.* 2015, 54, 1770–1774.
- [31] Kuo, W. S.; Chang, Y. T.; Cho, K. C.; Chiu, K. C.; Lien, C. H.; Yeh, C. S.; Chen, S. J. Gold nanomaterials conjugated with indocyanine green for dual-modality photodynamic and photothermal therapy. *Biomaterials* 2012, 33, 3270–3278.
- [32] Vankayala, R.; Huang, Y. K.; Kalluru, P.; Chiang, C. S.; Hwang, K. C. First demonstration of gold nanorods-mediated photodynamic therapeutic destruction of tumors via near infra-red light activation. *Small* 2014, 10, 1612–1622.
- [33] Zhao, T. T.; Shen, X. Q.; Li, L.; Guan, Z. P.; Gao, N. Y.; Yuan, P. Y.;

- Yao, S. Q.; Xu, Q. H.; Xu, G. Q. Gold nanorods as dual photo-sensitizing and imaging agents for two-photon photodynamic therapy. *Nanoscale* **2012**, *4*, 7712–7719.
- [34] Vankayala, R.; Lin, C. C.; Kalluru, P.; Chiang, C. S.; Hwang, K. C. Gold nanoshells-mediated bimodal photodynamic and photothermal cancer treatment using ultra-low doses of near infrared light. *Biomaterials* 2014, 35, 5527–5538.
- [35] Vijayaraghavan, P.; Liu, C. H.; Vankayala, R.; Chiang, C. S.; Hwang, K. C. Designing multi-branched gold nanoechinus for NIR light activated dual modal photodynamic and photothermal therapy in the second biological window. *Adv. Mater.* 2014, 26, 6689–6695.
- [36] Lin, J.; Wang, S. J.; Huang, P.; Wang, Z.; Chen, S. H.; Niu, G.; Li, W. W.; He, J.; Cui, D. X.; Lu, G. M. et al. Photosensitizer-loaded gold vesicles with strong plasmonic coupling effect for imaging-guided photothermal/photodynamic therapy. ACS Nano 2013, 7, 5320–5329.
- [37] Kim, Y. K.; Na, H. K.; Kim, S.; Jang, H. J.; Chang, S. J.; Min, D. H. One-pot synthesis of multifunctional Au@ graphene oxide nanocolloid core@ Shell nanoparticles for raman bioimaging, photothermal, and photodynamic therapy. Small 2015, 11, 2527–2535.